frontiers | Frontiers in Physics

TYPE Original Research
PUBLISHED 27 June 2025
DOI 10.3389/fphy.2025.1586773

OPEN ACCESS

EDITED BY
Luis M. Nieto,
University of Valladolid, Spain

REVIEWED BY
Outmane Oubram,
Universidad Autónoma del Estado de Morelos, Mexico
Sara Cruz Y. Cruz,
National Polytechnic Institute (IPN), Mexico

*CORRESPONDENCE
D. Martínez,
dunmar01@ucm.es

RECEIVED 03 March 2025
ACCEPTED 10 June 2025
PUBLISHED 27 June 2025

CITATION
Martínez D, Ruano PLA, Baba Y, Arroyo-Gascón O and Domínguez-Adame F (2025) Coherent potential approximation for disordered narrow-gap semiconductor superlattices.
Front. Phys. 13:1586773.
doi: 10.3389/fphy.2025.1586773

Coherent potential approximation for disordered narrow-gap semiconductor superlattices

D. Martínez[1]*, P. L. Alcázar Ruano[1], Y. Baba[2], O. Arroyo-Gascón[3] and F. Domínguez-Adame[1]

[1]GISC Departamento de Física de Materiales, Universidad Complutense, Madrid, Spain, [2]Departamento de Física Teórica de la Materia Condensada, Universidad Autónoma, Madrid, Spain, [3]Nanotechnology Group, USAL-Nanolab, Universidad de Salamanca, Salamanca, Spain

We introduce a solvable two-band model to study electron energy levels in disordered narrow-gap semiconductor superlattices within the $\boldsymbol{k}\cdot\boldsymbol{p}$ approach. The interaction of electrons with the impurities is accounted for by a separable pseudo-potential method that allows us to obtain closed expressions for the configurationally averaged Green's function using the coherent potential approximation. This approximation is regarded as the best single-site scattering theory to calculate the average spectral properties of disordered systems. As a working example, we focus on superlattices based on IV-VI compound semiconductors and present a thorough study of the configurationally averaged density of states. Our results are compared with the predictions of a single-band model and we conclude that the latter underestimates the density of states close to the band edge.

KEYWORDS

Dirac equation, Kronig-Penney model, non-local pseudopotential, disorder, coherent potential approximation

1 Introduction

The Dirac equation, formerly proposed almost a century ago as a relativistic quantum description for elementary spin–1/2 particles [1, 2], has recently attracted a lot of interest in the realm of condensed matter physics [3–5]. Relativistic corrections, arising from the Dirac equation after Taylor expansion in the particle velocity in units of the speed of light, such as spin-obit interaction and the Darwin term, can lead to an inversion of the normal ordering of electron bands in insulating materials containing heavy elements. As an example, semiconductor compounds $Pb_{1-x}Sn_xTe$ [6–8] and $Pb_{1-x}Sn_xSe$ [9] undergo an inversion of their L_6^+ and L_6^- bands as the Sn fraction is increased. The evolution of the bands indicates a gap closure at the L points of the Brillouin zone when a critical value of the Sn fraction is reached, signalling the occurrence of a phase transition from trivial to topological insulator. Topological insulators host gapless edge or surface states whose energy lies in the gap of the bulk material, thus enabling electron conduction through these surface states. Other examples of three dimensional topological insulators are BiSb, Bi_2Se_3, Bi_2Te_3 and strained HgTe, to mention a few (see Refs. [10–12] for reviews on the topic). Remarkably, effective Hamiltonians for topological states in three dimensional

topological insulators resemble the Dirac Hamiltonian [13], where the speed of light is replaced by a matrix element that takes into account the coupling between conduction-band and valence-band electron states of the bulk semiconductor. In many situations of interest, the effective Hamiltonians need to be corrected by including quadratic terms in momentum that are absent in the Dirac equation for relativistic electrons (see Ref. [3] for a thorough discussion).

The $\boldsymbol{k}\cdot\boldsymbol{p}$ perturbation approach for calculating the band structure of semiconductors [14–16] turns out to be another scenario where effective Hamiltonians with the same mathematical structure of the Dirac equation play a relevant role. To be specific, the matrix elements of the momentum operator between conduction-band and valence-band electron states cannot be neglected in narrow-gap semiconductors and at least two bands are needed in the expansion of the electron wave function in terms of the products of (slowly varying) envelope functions and (rapidly varying) Bloch functions. The resulting effective Hamiltonian acting upon the envelope functions in a two-band model for narrow-gap semiconductors is formally identical to the Dirac equation [17]. In this paper, we focus on the electron states close to the band edges in disordered narrow-gap semiconductor superlattices within the $\boldsymbol{k}\cdot\boldsymbol{p}$ approach. While the solution of the problem is straightforward in the case of perfectly periodic superlattices for various types of quantum well profiles (square [17], sawtooth [18], δ-doped [19]), real superlattices present unintentional disorder that breaks translational symmetry and Bloch's theorem does not hold [20, 21]. In addition, intentionally disordered superlattices have also been studied in the context of Anderson localization [22–24].

Green's function techniques are routinely used to obtain single-particle spectral properties of disordered matter, such as the density of states (DOS). We introduce a solvable two-band model of narrow-gap semiconductor superlattices to obtain the configurationally averaged Green's function of disordered narrow-gap semiconductor superlattices within the so-called coherent potential approximation (CPA). The CPA is an excellent and accurate alternative to purely numerical calculations [25–28]. Furthermore, particularly simple expressions for the configurationally averaged Green's function are achieved when the interaction of the electron with the superlattice is replaced by a separable pseudo-potential model [29–38]. In spite of its seemingly more complicated form, the separable pseudo-potential model is amenable to analytical solution and allows us to obtain closed expressions for the average Green's function within the CPA framework.

2 Theoretical model

Let us consider a superlattice consisting of alternating layers of two narrow-gap semiconductors, e.g., PbTe/PbSnTe [39], grown along the x axis. The envelope functions $f_c(x)$ and $f_v(x)$ describing conduction-band and valence-band states obey the following equation [17, 40].

$$\left[-i\hbar v\sigma_x\frac{\mathrm{d}}{\mathrm{d}x}+V(x)+\frac{1}{2}\sigma_z E_g(x)-E\right]\boldsymbol{\psi}(x)=0,\ \boldsymbol{\psi}(x)=\begin{pmatrix}f_c(x)\\ f_v(x)\end{pmatrix}, \quad (1)$$

where spatial derivatives of higher order are not considered, and σ_x and σ_z are Pauli matrices. Here, $E_g(x)$ is the position-dependent gap and $V(x)$ is the energy of the gap center. v is a parameter with dimensions of velocity related to the Kane's momentum matrix elements [16]. In our model we will assume that the interfaces are perfectly flat so that the momentum parallel to the interfaces $\boldsymbol{k}_\parallel$ is a constant of motion. We set $\boldsymbol{k}_\parallel = 0$ hereafter, although finite values of $\boldsymbol{k}_\parallel$ could be considered if needed.

In semiconductor superlattices, both the position-dependent gap $E_g(x)$ and the gap center $V(x)$ are piecewise functions of the spatial coordinate along the growth direction, corresponding to the semiconductor layers composing the system. In order to obtain a solvable model, we replace the interaction of the electron with the superlattice by a separable pseudo-potential model [29–38]. Hence, we perform the following substitution in Equation 1.

$$\left[V(x)+\frac{1}{2}\sigma_z E_g(x)\right]\boldsymbol{\psi}(x)\rightarrow\Delta\sigma_z\boldsymbol{\psi}(x)+\sum n\lambda_n\omega(x-na)\int_{-\infty}^{\infty}\omega(x'-na)\boldsymbol{\psi}(x')\mathrm{d}x', \quad (2a)$$

where the index n labels the semiconductor layers of width a. 2Δ is a reference gap that it is taken out from the summation for convenience. For the sake of brevity in the notation, we introduced the following 2×2 diagonal matrices

$$\lambda_n = V_n+\sigma_z\Delta_n. \quad (2b)$$

Here V_n is the energy of the gap center of the nth semiconductor layer. Similarly, $2\Delta_n$ is the difference of the gap of the nth layer and the reference gap 2Δ. $\omega(x)$ will be referred to as shape function hereafter. Remarkably, the introduction of the separable pseudo-potential model allows us to obtain closed solutions for any arbitrary shape function. Hence, we can set up an appropriate shape function that reproduces the observed energy spectrum of the considered system. Typically naive functions with very few adjustable parameters are good candidates [32, 34]. Within the framework of strongly coupled semiconductor superlattices, the dynamics of an electron in a potential well can be accurately described by a Dirac δ-type potential, following the approach introduced by Kronig and Penney [41]. This limiting case will be considered in our subsequent calculations below.

In a disordered superlattice, V_n and Δ_n are random variables with a given probability distribution function $\mathcal{P}(V_n,\Delta_n)$. In this work we will restrict ourselves to binary disorder with two different layers labeled A and B, for which the corresponding probability distribution is

$$\mathcal{P}(V_n,\Delta_n)=c\delta(V_n-V_\mathrm{A})\delta(\Delta_n-\Delta_\mathrm{A})+(1-c)\delta(V_n-V_\mathrm{B})\delta(\Delta_n-\Delta_\mathrm{B}),$$

where c is the fraction of A layers in the superlattice. This type of probability distribution corresponds to intentionally disordered superlattices where the individual layer thicknesses take on two values at random [20, 22, 24]. Other models of disorder can be addressed on the same footing by selecting an appropriate probability distribution, such as the Gaussian function introduced in Anderson's seminal paper [42]. Nevertheless, in this study we concentrate on the case of binary disorder as a representative example for the application of the CPA.

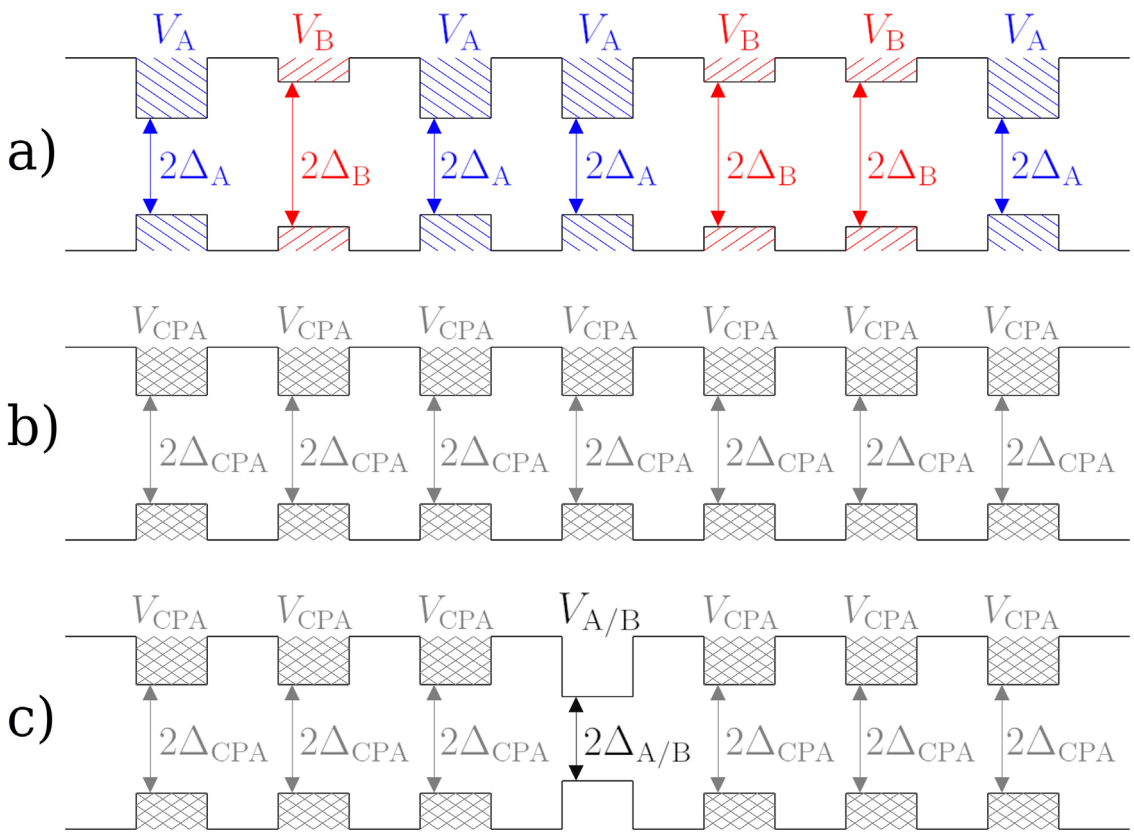

FIGURE 1
(a) A realization of the disordered superlattice, illustrating the conduction- and valence-band edge profiles along with the band gaps of the two constituent layers. In our model, the actual band-edge profile is substituted by a nonlocal pseudopotential in the Dirac-like equation for the envelope functions (1). **(b)** The effective superlattice, constructed to compute the average Green's function, is translationally invariant and described by the complex parameters V_{CPA} and Δ_{CPA}. **(c)** The self-consistency condition is established by replacing one of the layers in the effective superlattice with a layer (A or B) of the disordered superlattice, and requiring that the single-site t−matrix vanishes.

3 Coherent potential approximation

Configurationally averaged spectral properties of random systems cannot be calculated exactly in most cases and suitable approximations are needed. Among them, the CPA stands out as the best single-site theory for the study of the spectral properties of disordered systems [43–52]. The starting point is the (retarded) resolvent of a given random Hamiltonian H, formally defined as $\widehat{G}(z) \equiv (z - \widehat{H})^{-1}$ with $z \equiv E + i0^+$, where 0^+ is a small positive quantity which is allowed to vanish after mathematical operations. Our interest concerns the average of the resolvent over the possible configurations of the disorder, $\langle \widehat{G}(z) \rangle_{av} = \int \mathcal{P}(V_n, \Delta_n) \widehat{G}(z) \mathrm{d}V_n \mathrm{d}\Delta_n$, from which the average DOS can be readily obtained. The CPA combines two basic ideas. On one side, the average resolvent of the random system (see Figure 1a) is calculated by introducing a periodic (translationally invariant) effective medium. On the other hand, this effective medium is determined by demanding that the fluctuations of the resolvent average out to zero, thus leading to a self-consistency condition [28].

Following the proposal by Sievert and Glasser [30], we will assume that the effective medium is characterized by a uniform gap (see Figure 1b) and replace $\lambda_n = V_n + \sigma_z \Delta_n$ by $\lambda_{CPA} \equiv V_{CPA} + \sigma_z \Delta_{CPA}$ in the corresponding Equation 2a for this translational invariant medium. The two parameters V_{CPA} and Δ_{CPA} are complex in general and play the same role as the coherent potential in the conventional CPA. The parameters of the effective medium will be determined by a self-consistency condition [28]. This is performed in practice by substituting one of the potential terms in the two-band model equation for the effective medium by a potential with coupling constant $V_{A/B} + \sigma_z \Delta_{A/B}$ (see Figure 1c) and nullifying the single-site t–matrix. After performing the average with the probability distribution function (3), the self-consistency equation reads (see Ref. [30] for details).

$$(\lambda_{CPA} - \lambda_A)\mathcal{F}(z, \lambda_{CPA})(\lambda_{CPA} - \lambda_B) + \lambda_{CPA} - \lambda_{VCA} = 0, \tag{3a}$$

where

$$\lambda_{VCA} = c\lambda_A + (1 - c)\lambda_B \tag{3b}$$

is the virtual crystal approximation value [28] and

$$\mathcal{F}(z, \lambda_{CPA}) = \int_{-\infty}^{\infty} \int_{-\infty}^{\infty} \omega(x)\, \omega(x')\, G_{eff}(x, x'; z)\, \mathrm{d}x \mathrm{d}x'. \tag{3c}$$

Here, $G_{eff}(x, x'; z)$ denotes the Green's function of the effective medium. Since this medium is translationally invariant, the Green's function actually depends on the difference $x - x'$, but we will keep

the standard notation. Equation 3a is an implicit equation for the two unknowns V_{CPA} and Δ_{CPA} that can be solved iteratively if $G_{\mathrm{eff}}(x,x';z)$ is known.

4 Green's function of the effective medium

To proceed, we need to calculate the Green's function of the effective medium. Therefore, we look for the solution of the following equation

$$\left(-i\hbar v\sigma_x\frac{\partial}{\partial x}+\Delta\sigma_z-z\right)G_{\mathrm{eff}}(x,x';z)+\lambda_{\mathrm{CPA}}\sum_n\omega(x-na)\times\int_{-\infty}^{\infty}\omega(x''-na)\,G_{\mathrm{eff}}(x'',x';z)\,\mathrm{d}x''=-\delta(x-x').$$

We now Fourier transform with respect to the x coordinate and obtain

$$(\hbar vk\sigma_x+\Delta\sigma_z-z)\,\widetilde{G}_{\mathrm{eff}}(k,x';z)+\lambda_{\mathrm{CPA}}\int_{-\infty}^{\infty}\left(\sum_n e^{i(q-k)na}\right)\widetilde{\omega}(k)\times\widetilde{\omega}^*(q)\,\widetilde{G}_{\mathrm{eff}}(q,x';z)\,\mathrm{d}q=-\frac{1}{\sqrt{2\pi}}e^{-ikx'}. \quad (4)$$

Here $\widetilde{f}(q)=(1/\sqrt{2\pi})\int_{-\infty}^{\infty}\exp(-iqx)\,f(x)\,\mathrm{d}x$ denotes the Fourier transform of the function $f(x)$. We assume $\omega(x)$ to be a real function and consequently $\widetilde{\omega}(-q)=\widetilde{\omega}^*(q)$.

Calculations are largely simplified assuming that the range of the shape function is non-zero and hence its Fourier transform vanishes outside the first Brillouin zone $[-\pi/a,\pi/a]$, as pointed out by Sievert and Glasser [30]. This can be understood by inspection of the summation over n appearing in Equation 4, which is nonzero only if k and q differ by a reciprocal wave number. The summation is multiplied by the product $\widetilde{\omega}(k)\;\;\widetilde{\omega}^*(q)$ that vanishes unless both k and q belong to the first Brillouin zone. Whence

$$\left(\sum_n e^{i(q-k)na}\right)\widetilde{\omega}(k)\,\widetilde{\omega}^*(q)=\frac{2\pi}{a}|\widetilde{\omega}(k)|^2\delta(q-k),$$

when $\widetilde{\omega}(k)=0$ for $|k|>\pi/a$. Inserting this result into Equation 4 to obtain $\widetilde{G}_{\mathrm{eff}}(k,x';z)$ and performing the inverse Fourier transform yields

$$G_{\mathrm{eff}}(x,x';z)=\frac{1}{2\pi}\int_{-\infty}^{\infty}e^{ik(x-x')}\left[z-\hbar vk\sigma_x-\Delta\sigma_z-2\pi\frac{\lambda_{\mathrm{CPA}}}{a}|\widetilde{\omega}(k)|^2\right]^{-1}\mathrm{d}k. \quad (5)$$

Therefore

$$\mathcal{F}(z,\lambda_{\mathrm{CPA}})=\int_{-\infty}^{\infty}|\widetilde{\omega}(k)|^2\left[z-\hbar vk\sigma_x-\Delta\sigma_z-2\pi\frac{\lambda_{\mathrm{CPA}}}{a}|\widetilde{\omega}(k)|^2\right]^{-1}\mathrm{d}k. \quad (6)$$

We will consider functions $\widetilde{\omega}(k)$ with well-defined parity hereafter without loss of generality. Thus, $|\widetilde{\omega}(k)|^2$ in Equation 6 is an even function of the wave number k. It is straightforward to demonstrate that in this case the off-diagonal terms of the 2×2 matrix appearing in the integrand are odd functions of k and vanish after integration. Hence, $\mathcal{F}(z,\lambda_{\mathrm{CPA}})$ turns out to be a 2×2 diagonal matrix. Recalling that $\lambda_{\mathrm{CPA}}=V_{\mathrm{CPA}}+\sigma_z\Delta_{\mathrm{CPA}}$ we get the following expression

$$\mathcal{F}(z,\lambda_{\mathrm{CPA}})=\int_{-\infty}^{\infty}|\widetilde{\omega}(k)|^2\left[z-2\pi\frac{V_{\mathrm{CPA}}}{a}|\widetilde{\omega}(k)|^2+\left(\Delta+2\pi\frac{\Delta_{\mathrm{CPA}}}{a}|\widetilde{\omega}(k)|^2\right)\sigma_z\right]\times\left[\left(z-2\pi\frac{V_{\mathrm{CPA}}}{a}|\widetilde{\omega}(k)|^2\right)^2-\left(\Delta+2\pi\frac{\Delta_{\mathrm{CPA}}}{a}|\widetilde{\omega}(k)|^2\right)^2-\hbar^2v^2k^2\right]^{-1}\mathrm{d}k, \quad (7)$$

that inserted back into Equation 3a yields two scalar coupled equations for the two unknowns V_{CPA} and Δ_{CPA} that can be solved by self-consistent methods.

Once the Green's function of the effective medium is obtained, relevant physical quantities can be calculated. In particular, the average DOS per unit length is easily computed by the following expression

$$\rho(E)=-\frac{1}{\pi L}\mathrm{Im}\left[\mathrm{Tr}\left(\widehat{G}_{\mathrm{eff}}(E+i0^+)\right)\right]=-\frac{1}{\pi}\mathrm{Im}\left[\mathrm{Tr}\left(G_{\mathrm{eff}}(0,0;E+i0^+)\right)\right], \quad (8)$$

where $L\gg a$ is the system length. Besides the DOS, the knowledge of the Green's function allows us to calculate the electric conductivity in the linear response approximation [28] or the optical absorption spectrum [53].

5 Wide-gap limit

Electron states of wide-gap semiconductor superlattices are accurately described within a single band approach, known as BenDaniel-Duke model [54]. In this model, the envelope-function of the conduction (or valence) band states satisfies a Schrödinger-like equation where the bare electron mass is replaced by a position-dependent effective mass $m^*(x)$. In this section we consider the applicability of our two-band model to study disordered wide-gap semiconductor superlattices. This limiting case corresponds to $\Delta,v\to\infty$ in such a way that the effective mass $m^*=\Delta/v^2$ remains finite. Notice that we are considering $\Delta_n=0$ for simplicity and consequently the effective mass is the same in the two semiconductor layers.

Let us define $z_{\mathrm{wg}}=z-\Delta$ to shift the origin of energy from the gap center to the conduction band edge. We are interested in the states near the band edge and take $|z_{\mathrm{wg}}|\ll\Delta$ in what follows. At moderate magnitude of disorder we also assume $|\Delta_{\mathrm{CPA}}\|\widetilde{\omega}(k)|^2/a\ll\Delta$ in the wide-gap limit. Therefore, from Equation 7 we easily see that $\mathcal{F}_{22}/\mathcal{F}_{11}$ is of the order of $|z_{\mathrm{wg}}|/\Delta\ll1$ so that $\mathcal{F}_{22}$ can be disregarded and

$$\mathcal{F}_{11}(z_{\mathrm{wg}},\lambda_{\mathrm{CPA}})\simeq\int_{-\infty}^{\infty}|\widetilde{\omega}(k)|^2\left(z_{\mathrm{wg}}-2\pi\frac{V_{\mathrm{CPA}}}{a}|\widetilde{\omega}(k)|^2-\frac{\hbar^2v^2}{2\Delta}k^2\right)^{-1}\mathrm{d}k.$$

This results agrees with that obtained in Reference [30] after the substitution $\hbar^2v^2/2\Delta\to\hbar^2/2m^*$.

6 Results

Notice that Equation 7 is valid for any Fourier transform of the shape function. In this work we set a top-hat function as a working example, but the general conclusions are valid for other functions

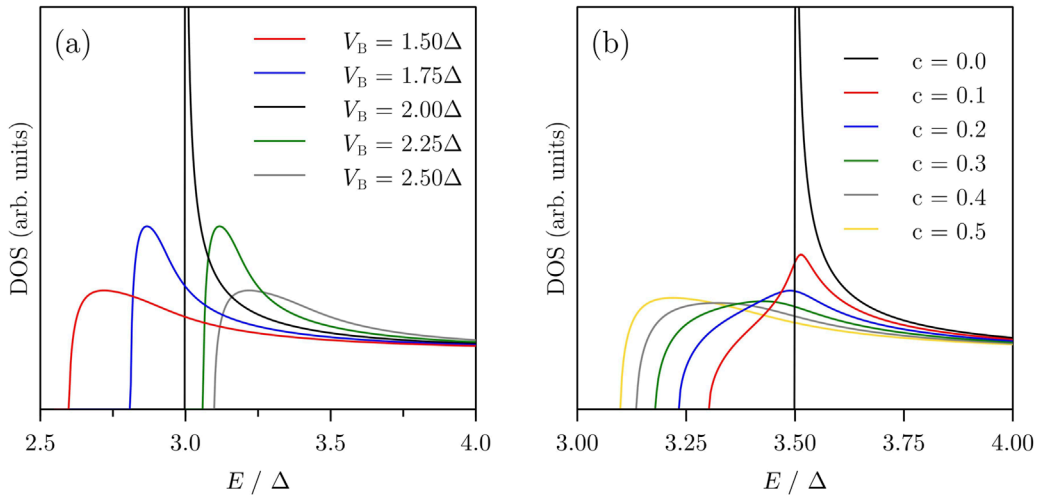

FIGURE 2
Average DOS in arbitrary units as a function of energy E expressed in units of Δ for **(a)** various values of the energy of the gap center in the B layers V_B when $V_A = 2\Delta$ and $c = 0.5$, and **(b)** various values of the fraction c of A layers when $V_A = 2\Delta$ and $V_B = 2.5\Delta$. In all cases $\Delta_A = \Delta_B = 0$.

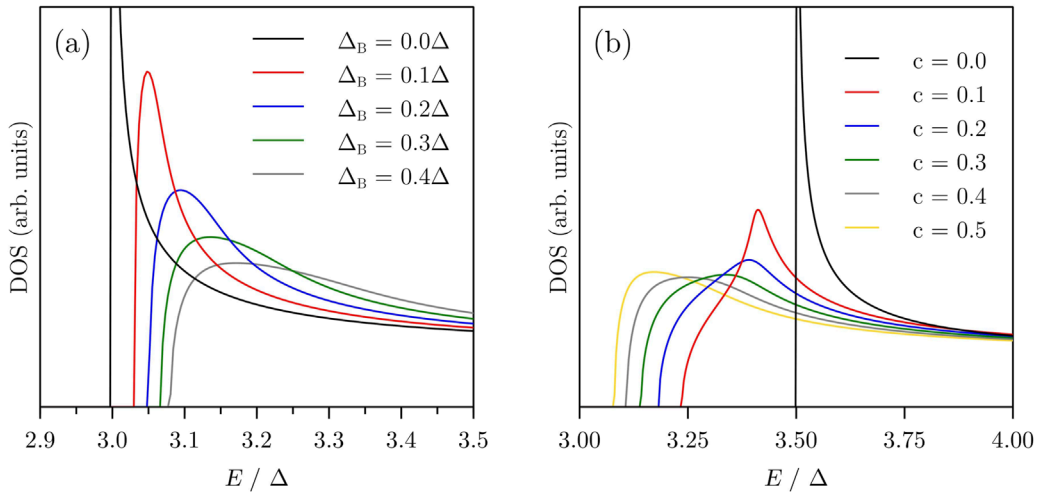

FIGURE 3
Average DOS in arbitrary units as a function of energy E expressed in units of Δ for **(a)** various values of Δ_B when $c = 0.5$ and **(b)** various values of the fraction c of A layers when $\Delta_B = 0.4\Delta$. In all cases $\Delta_A = 0$, $V_A = V_B = 2\Delta$.

$$\widetilde{\omega}(k) = \sqrt{\frac{a}{2\pi}}\theta(k_c - |k|),$$

where θ is the Heaviside step-function and k_c is a momentum cutoff to ensure that $\widetilde{\omega}(k)$ vanishes outside the first Brillouin zone. To avoid the profusion of free parameters, we fix $k_c = \pi/a$ in what follows. Finally, from Equations 5 and 8, the configurationally averaged DOS per unit length reads

$$\rho(E) = -\frac{2}{\pi^2}(E - V_{\mathrm{CPA}})\,\mathrm{Im}\int_0^{\pi/a}\left[(E + i0^+ - V_{\mathrm{CPA}})^2 - (\Delta + \Delta_{\mathrm{CPA}})^2 - \hbar^2 v^2 k^2\right]^{-1} \mathrm{d}k\ .$$

As an application of our results, we will focus on typical values of the model parameters for IV-VI compound semiconductors. Hence, we take $\Delta = 75$meV and $\hbar v/\Delta = 4.5$nm. It is therefore more convenient to define the following dimensionless parameter $\beta = (\hbar v/a\Delta)^2$, being $\beta = 2.25$ for $a = 3$nm. To estimate representative values of V_A and V_B in superlattices of IV-VI compound semiconductors, we consider a single term in Equation 2a, say $n = 0$, and solve the corresponding two-band model equation. For positive values of V_0 the single-layer potential binds a hole with energy E_0. Straightforward calculations lead to $V_0/\Delta = \sqrt{4\beta(\Delta + E_0)/(\Delta - E_0)}$ (in the limit $k_c \to \infty$ for simplicity). Considering a particular value of the acceptor energy level of 20meV above the edge of the valence band, then we find $E_0 = -55$meV with respect to the gap center and consequently $V_0 \simeq 1.8\,\Delta$.

After discussing suitable values of the model parameters for IV-VI compound semiconductors, we present the results for the configurationally averaged DOS per unit length Equation 8. We start

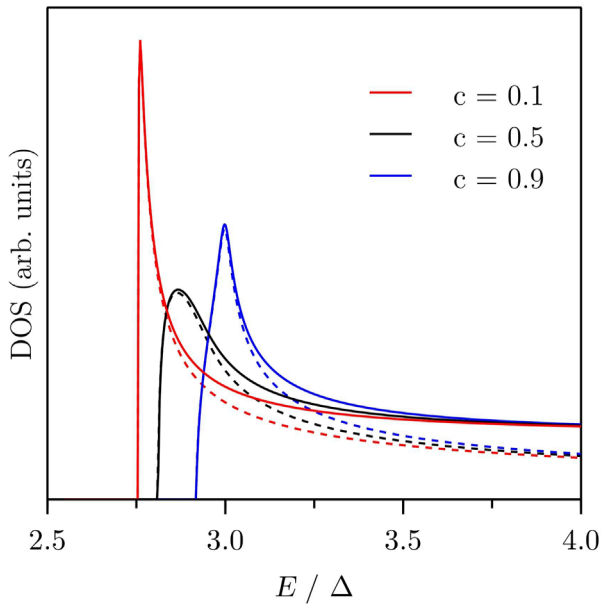

FIGURE 4
Average DOS in arbitrary units as a function of energy E expressed in units of Δ for various values of the fraction c of A layers when V_A = 1.75Δ and V_B = 2Δ. Solid (dashed) lines correspond to the two-band (single-band) model.

by analyzing the impact of the disorder arising from a random binary distribution of gap centers, setting $\Delta_n = 0$ for the moment. In this case, it is most important to notice that the results depend only on the difference $\delta V \equiv V_A - V_B$ when the DOS is plotted as a function of $\bar{E} \equiv E - V_{VCA}$ with $V_{VCA} = cV_A + (1-c)V_B$. This symmetry is easily proven by defining $\bar{V} \equiv V_{CPA} - V_{VCA}$ and noticing that the self-consistency Equation 3a can be rewritten as

$$(\bar{V} - (1-c)\,\delta V)\,\mathcal{F}(\bar{E} + i0^+, \bar{V})\,(\bar{V} + c\delta V) + \bar{V} = 0\ . \tag{9}$$

In addition, Equation 9 is invariant under the simultaneous change $\delta V \to -\delta V$ and $c \to 1 - c$. As a consequence, we can set c in the range [0,0.5] hereafter.

In Figure 2a we plot the average DOS in arbitrary units as a function of energy E (expressed in units of Δ) for various values of the gap center energy of the B layers V_B when $V_A = 2\Delta$ and $c = 0.5$. We fix the same value $\beta = 2.25$ for all calculations. The DOS turns out to be symmetric around the center of the gap of the effective medium and, for this reason, only the DOS in the conduction band is depicted. The DOS of the ordered superlattice, namely, $V_B = 2\Delta$, displays a divergence at the band edge, as expected (recall that the momentum parallel to the interfaces is set to zero and consequently the DOS corresponds to a one-dimensional system). In disordered superlattices, the divergence is smeared out and the band edge shifts in energy upwards (downwards) when V_B is smaller (larger) than V_A. In addition, the peak of the DOS around the band edge becomes broader and the gap of the effective medium shrinks (not shown) upon increasing $|\delta V|$. Figure 2b shows the DOS as a function of energy for various values of the fraction c of A layers when $V_A = 2\Delta$ and $V_B = 2.5\Delta$. We notice that the band edge shifts to lower energy on increasing c, consistent with the fact that $V_A < V_B$.

Having discussed the salient features of the DOS when disorder originates from the shift of the gap centers in the semiconductors A and B, we now turn our attention to the situation $\Delta_n \neq 0$ while keeping V_n constant. Figure 3a depicts the average DOS in arbitrary units as a function of energy E (expressed in units of Δ) for various values of Δ_B when $\Delta_A = 0$, $V_A = V_B = 2\Delta$ and $c = 0.5$. We observe that the conduction band states are pushed upwards and the maximum of the DOS becomes broader on increasing Δ_B. Figure 3b demonstrates that the conduction band edge shifts to lower energies when the fraction of A layers increases, following a similar trend to that found in Figure 2b.

Finally, we compare our results with the predictions of the single-band model discussed in Section 5. In the wide-gap limit, the configurationally averaged DOS per unit length (14) reduces to

$$\rho(E) \simeq -\frac{1}{\pi^2}\,\mathrm{Im}\int_0^{\pi/a}\left(E + i0^+ - \Delta - V_{CPA} - \frac{\hbar^2 v^2}{2\Delta}k^2\right)^{-1}\mathrm{d}k.$$

Figure 4 compares the results obtained with the two-band model (solid lines) and the single-band model (dashed lines) for several values of the of the fraction c of A layers when $V_A = 1.75\Delta$ and $V_B = 2\Delta$. We observe an increase of the configurationally averaged DOS at the high-energy side of the peaks in the two-band model compared to the wide-gap limit. We attribute this enhancement to non-parabolicity effects arising in the two-band model. Specifically, the bands of the effective medium flatten upon increasing energy, an effect that it is more pronounced in narrow-gap semiconductors and it can be viewed as an increase of the effective mass. Since the DOS in one-dimensional systems is proportional to the square root of the effective mass, non-parabolicity effects reflect themselves as an enhancement of the DOS upon increasing energy.

7 Conclusion

We have introduced a solvable model for random narrow-gap semiconductor superlattices where two type of layers of the same width are arranged at random along the growth direction. In the $\boldsymbol{k}\cdot\boldsymbol{p}$ approximation framework, the interband matrix element of narrow-gap semiconductors, parameterized by v, is not negligible and at least two bands are needed to accurately describe the electronic states. The average spectral properties have been calculated with a reliable implementation of the CPA after introducing a separable pseudo-potential. We have demonstrated that the two-band model predictions are in agreement with the results derived by a single-band model [30] after letting the gap be the largest energy scale of the problem. We used our model to study the impact of the disorder on the electron states in superlattices of narrow-gap IV-VI compound semiconductors when the center of the gap or the magnitude of the gap of each layer are random variables with a binary probability distribution.

It is worth noticing that the validity of our approach is not restricted to the field of condensed matter physics. Equation 1 for a periodic array of local δ-function potentials is the well-known Dirac-Kronig-Penney model that McKellar and Stephenson proposed as a crude approximation to describe the relativistic dynamics of quarks in the nucleus [55, 56]. The use of separable pseudo-potentials (2a) would allow to deal with more elaborated and

realistic interaction potentials. Moreover, demanding periodicity seems too restrictive to describe the nucleus, and the introduction of disorder would improve those relativistic models which, in the end, can be tackled with the same techniques presented in this work.

Data availability statement

The raw data supporting the conclusions of this article will be made available by the authors, without undue reservation.

Author contributions

DM: Data curation, Formal Analysis, Investigation, Software, Writing – review and editing. PR: Data curation, Formal Analysis, Investigation, Software, Writing – review and editing. YB: Conceptualization, Supervision, Validation, Writing – review and editing. OA-G: Conceptualization, Supervision, Validation, Writing – review and editing, Formal Analysis. FD-A: Conceptualization, Formal Analysis, Funding acquisition, Methodology, Visualization, Writing – original draft, Writing – review and editing.

Funding

The author(s) declare that financial support was received for the research and/or publication of this article. This work was supported by the "(MAD2D-CM)-UCM" project funded by Comunidad de Madrid, by the Recovery, Transformation and Resilience Plan, and by NextGenerationEU from the European Union and Agencia Estatal de Investigación of Spain (Grant PID2022-136285NB-C31).

Acknowledgments

The authors acknowledge M. García, R. Molina and A. López for helpful discussions.

Conflict of interest

The authors declare that the research was conducted in the absence of any commercial or financial relationships that could be construed as a potential conflict of interest.

Generative AI statement

The author(s) declare that no Generative AI was used in the creation of this manuscript.

Publisher's note

References

1. Dirac PAM. The quantum theory of the electron. *Proc R Soc Lond A* (1928) 117:610. doi:10.1098/rspa.1928.0023

2. Thaller B. *The Dirac equation*. New York: Springer-Verlag (1992).

3. Shen SQ. Topological insulators. In: *Dirac equation in condensed matters*. New York: Springer-Verlag (2012).

4. Wehling T, Black-Schaffer A, Balatsky A. Dirac materials. *Dirac Materials Adv Phys* (2014) 63:1–76. doi:10.1080/00018732.2014.927109

5. Vafek O, Vishwanath A. Dirac fermions in solids: from high-T_c cuprates and graphene to topological insulators and weyl semimetals. *Annu Rev Condens Matter Phys* (2014) 5:83–112. doi:10.1146/annurev-conmatphys-031113-133841

6. Hsieh TH, Lin H, Li J, Duan W, Bansil A, Fu L. Topological crystalline insulators in the SnTe material class. *Nat Commun* (2012) 3:982. doi:10.1038/ncomms1969

7. Xu SY, Liu C, Alidoust N, Neupane M, Qian D, Belopolski I, et al. Observation of a topological crystalline insulator phase and topological phase transition in $Pb_{1-x}Sn_xTe$. *Nat Comm* (2012) 7:12505. doi:10.1038/ncomms12505

8. Assaf BA, Phuphachong T, Volobuev VV, Inhofer A, Bauer G, Springholz G, et al. Massive and massless Dirac fermions in $Pb_{1-x}Sn_xTe$ topological crystalline insulator probed by magneto-optical absorption. *Sci Rep* (2016) 6:20323. doi:10.1038/srep20323

9. Dziawa P, Kowalski BJ, Dybko K, Buczko R, Szczerbakow A, Szot M, et al. Topological crystalline insulator states in $Pb_{1-x}Sn_xSe$. *Nat Mater* (2012) 11:1023–7. doi:10.1038/nmat3449

10. Fruchart M, Carpentier D. An introduction to topological insulators. *C R Phys* (2013) 14:779–815. doi:10.1016/j.crhy.2013.09.013

11. Ando Y. Topological insulator materials. *J Phys Soc Jpn* (2013) 82:102001. doi:10.7566/jpsj.82.102001

12. Zhang H, Liu CX, Qi XL, Dai X, Fang Z, Zhang SC. Topological insulators in bi2se3, bi2te3 and sb2te3 with a single Dirac cone on the surface. *Nat Phys* (2009) 5:438–42. doi:10.1038/nphys1270

13. Hasan MZ, Kane CL. Colloquium: topological insulators. *Rev Mod Phys* (2010) 82:3045–67. doi:10.1103/revmodphys.82.3045

14. Parmenter RH. Symmetry properties of the energy bands of the zinc blende structure. *Phys Rev* (1955) 100:573–9. doi:10.1103/physrev.100.573

15. Dresselhaus G. Spin-orbit coupling effects in zinc blende structures. *Phys Rev* (1955) 100:580–6. doi:10.1103/physrev.100.580

16. Kane EO. Band structure of indium antimonide. *J Phys Chem Sol* (1957) 1:249–61. doi:10.1016/0022-3697(57)90013-6

17. Bastard G. *Wave mechanics applied to semiconductor heterostructures*. New Jersey: Wiley Interscience (1991).

18. Domínguez-Adame F, Méndez B. Sawtooth superlattices in a two-band semiconductor. *Semicond Sci Technol* (1994) 9:1358–62. doi:10.1088/0268-1242/9/7/010

19. Domínguez-Adame F. Subband energy in two-band delta-doped semiconductors. *Phys Lett A* (1996) 211:247–51. doi:10.1016/0375-9601(95)00976-0

20. Mäder KA, Wang L, Zunger A. Electronic consequences of random layer-thickness fluctuations in AlAs/GaAs superlattices. *J Appl Phys* (1995) 78:6639–57. doi:10.1063/1.360728

21. Miller MK, Diercks D, Brooks Tellekamp M. Improving luminescence response in ZnGeN2/GaN superlattices: defect reduction through composition control. *J Phys D Appl Phys* (2024) 57:375106. doi:10.1088/1361-6463/ad54ce

22. Chomette A, Deveaud B, Regreny A, Bastard G. Observation of carrier localization in intentionally disordered GaAs/GaAlAs superlattices. *Phys Rev Lett* (1986) 57:1464–7. doi:10.1103/physrevlett.57.1464

23. Pavesi L, Tuncel E, Zimmermann B, Reinhart FK. Photoluminescence of disorder-induced localized states in GaAs/$Al_xGa_{1-x}As$ superlattices. *Phys Rev B* (1989) 39:7788–95. doi:10.1103/physrevb.39.7788

24. Bellani V, Diez E, Hey R, Toni L, Tarricone L, Parravicini GB, et al. Experimental evidence of delocalized states in random dimer superlattices. *Phys Rev Lett* (1999) 82:2159–62. doi:10.1103/physrevlett.82.2159

25. Sen PN, Cohen MH. Two band model of a disordered semiconducting binary alloy in the coherent potential approximation. *J Non-cryst Sol* (1972) 8-10:147–54. doi:10.1016/0022-3093(72)90128-7

26. Jones W, March N. *Theoretical solid state physics: non-equilibrium and disorder*. New York: Dover Publications (1985).

27. Gonis A. *Green functions for ordered and disordered systems*. Amsterdam: North-Holland (1992).

28. Economou E. *Green's functions in quantum physics*. Berlin: Springer (2006).

29. Knight BW, Peterson GA. Solvable three-dimensional lattice models. *Phys Rev* (1963) 132:1085–92. doi:10.1103/physrev.132.1085

30. Sievert PR, Glasser ML. Interband effects in the coherent-potential approximation. I. *Phys Rev B* (1973) 7:1265–9. doi:10.1103/physrevb.7.1265

31. Glasser ML, Sievert PR. Interband effects in the coherent potential approximation: simple two band model. *Can J Phys* (1975) 53:1109–13. doi:10.1139/p75-140

32. Domínguez-Adame F, Méndez B, Maciá E, González MA. Non-local separable potential approach to multicentre interactions. *Mol Phys* (1991) 74:1065–9. doi:10.1080/00268979100102801

33. Domínguez-Adame F, González MA. A generalized Dirac-Kronig-Penney model with nonlocal separable potentials. *Phys B: Condens Matter* (1992) 176:180–8. doi:10.1016/0921-4526(92)90003-b

34. Domínguez-Adame F, Diez E, Sánchez A. Three-dimensional effects on extended states in disordered models of polymers. *Phys Rev B* (1995) 51:8115–24. doi:10.1103/physrevb.51.8115

35. de Prunelé E. Solvable model for three-dimensional quantum scattering of a particle off several separable interactions centred at n arbitrary points. *J Phys A Math Gen* (1997) 30:7831–48. doi:10.1088/0305-4470/30/22/021

36. López S, Domínguez-Adame F. Non-local potential approach to the ground state of confined excitons in quantum dots. *Semicon Sci Technol* (2002) 17:227. doi:10.1088/0268-1242/17/3/308

37. González-Santander C, Apostolova T, Domínguez-Adame F. Binding energy of hydrogenic impurities in quantum dots under intense laser radiation. *J Phys Condens Matter* (2013) 25:335802. doi:10.1088/0953-8984/25/33/335802

38. Hernando JL, Baba Y, Díaz E, Domínguez-Adame F. Many-impurity scattering on the surface of a topological insulator. *Sci Rep* (2021) 11:5810. doi:10.1038/s41598-021-84801-w

39. Bauer G. IV–VI compound compositional and doping superlattices. *Superlattices Microstruct.* (1986) 2:531–8. doi:10.1016/0749-6036(86)90111-4

40. Domínguez-Adame F, Maciá E, Méndez B. Fibonacci superlattices of narrow-gap III-V semiconductors. *Semicond Sci Technol* (1995) 10:797–802. doi:10.1088/0268-1242/10/6/009

41. de L Kronig R, Penney WG. Quantum mechanics of electrons in crystal lattices. *Proc Roy Soc (London) A* (1931) 130:499. doi:10.1098/rspa.1931.0019

42. Anderson PW. Absence of diffusion in certain random lattices. *Phys Rev* (1958) 109:1492–505. doi:10.1103/physrev.109.1492

43. Soven P. Coherent-potential model of substitutional disordered alloys. *Phys Rev* (1967) 156:809–13. doi:10.1103/physrev.156.809

44. Taylor DW. Vibrational properties of imperfect crystals with large defect concentrations. *Phys Rev* (1967) 156:1017–29. doi:10.1103/physrev.156.1017

45. Onodera Y, Toyozawa Y. Persistence and amalgamation types in the electronic structure of mixed crystals. *J Phys Soc Jpn* (1968) 24:341–55. doi:10.1143/jpsj.24.341

46. Velický B. Theory of electronic transport in disordered binary alloys: coherent-potential approximation. *Phys Rev* (1969) 184:614–27. doi:10.1103/physrev.184.614

47. Di Sante D, Barone P, Plekhanov E, Ciuchi S, Picozzi S. Robustness of rashba and Dirac fermions against strong disorder. *Sci Rep* (2015) 5:11285. doi:10.1038/srep11285

48. Eyméoud P, Maugis P. Magnetic behavior of transition metal solutes in α-iron: a classification. *J Magn Magn Mater* (2020) 513:167223. doi:10.1016/j.jmmm.2020.167223

49. Chadov S, Kiss J, Kübler J, Felser C. Topological phase transition in bulk materials described by the coherent potential approximation technique. *Phys Status Solidi - Rapid Res Lett* (2013) 7:82. doi:10.1002/pssr.201206395

50. Köhler S, Ruocco G, Schirmacher W. Coherent potential approximation for diffusion and wave propagation in topologically disordered systems. *Phys Rev B* (2013) 88:064203. doi:10.1103/physrevb.88.064203

51. Zainullina V, Korotin M, Kozhevnikov V. Electronic properties of disordered perovskite-like ferrites: coherent potential approach. *Prog Solid State Chem* (2020) 60:100284. doi:10.1016/j.progsolidstchem.2020.100284

52. Martin AM, Litak G, Györffy BL, Annett JF, Wysokiński KI. Coherent potential approximation for d-wave superconductivity in disordered systems. *Phys Rev B* (1999) 60:7523–35. doi:10.1103/physrevb.60.7523

53. Huber DL, Ching WY. Numerical simulation of the optical spectra of frenkel excitons in disordered systems. *Phys Rev B* (1989) 39:8652–6. doi:10.1103/physrevb.39.8652

54. BenDaniel DJ, Duke CB. Space-charge effects on electron tunneling. *Phys Rev* (1966) 152:683–92. doi:10.1103/physrev.152.683

55. McKellar BHJ, Stephenson GJ. Klein paradox and the Dirac-Kronig-Penney model. *Phys Rev A* (1987) 36:2566–9. doi:10.1103/physreva.36.2566

56. McKellar BHJ, Stephenson GJ. Relativistic quarks in one-dimensional periodic structures. *Phys Rev C* (1987) 35:2262–71. doi:10.1103/physrevc.35.2262